The Journal of Experimental Biology 216, 3709-3723

doi:10.1242/jeb.079665

RESEARCH ARTICLE

A three-dimensional musculoskeletal model of the chimpanzee (*Pan troglodytes*) pelvis and hind limb

Matthew C. O'Neill[1], Leng-Feng Lee[2], Susan G. Larson[1], Brigitte Demes[1], Jack T. Stern, Jr[1] and Brian R. Umberger[2,*]

[1]Department of Anatomical Sciences, Stony Brook University School of Medicine, Stony Brook, NY 11794, USA and
[2]Department of Kinesiology, University of Massachusetts Amherst, Amherst, MA 01003, USA

*Author for correspondence (umberger@kin.umass.edu)

SUMMARY

Musculoskeletal models have become important tools for studying a range of muscle-driven movements. However, most work has been in modern humans, with few applications in other species. Chimpanzees are facultative bipeds and our closest living relatives, and have provided numerous important insights into our own evolution. A chimpanzee musculoskeletal model would allow integration across a wide range of laboratory-based experimental data, providing new insights into the determinants of their locomotor performance capabilities, as well as the origins and evolution of human bipedalism. Here, we described a detailed three-dimensional (3D) musculoskeletal model of the chimpanzee pelvis and hind limb. The model includes geometric representations of bones and joints, as well as 35 muscle–tendon units that were represented using 44 Hill-type muscle models. Muscle architecture data, such as muscle masses, fascicle lengths and pennation angles, were drawn from literature sources. The model permits calculation of 3D muscle moment arms, muscle–tendon lengths and isometric muscle forces over a wide range of joint positions. Muscle–tendon moment arms predicted by the model were generally in good agreement with tendon-excursion estimates from cadaveric specimens. Sensitivity analyses provided information on the parameters that model predictions are most and least sensitive to, which offers important context for interpreting future results obtained with the model. Comparisons with a similar human musculoskeletal model indicate that chimpanzees are better suited for force production over a larger range of joint positions than humans. This study represents an important step in understanding the integrated function of the neuromusculoskeletal systems in chimpanzee locomotion.

Key words: chimpanzee, model, muscle, moment arm, force.

Received 3 September 2012; Accepted 2 June 2013

INTRODUCTION

Musculoskeletal models have become important tools for studying the mechanics, energetics and control of locomotion. Several human models have been developed (e.g. Delp et al., 1990; Hatze, 1977; Modenese et al., 2011), permitting predictions of muscle–tendon kinematics and moment arms across a range of three-dimensional (3D) joint positions. When combined with detailed muscle architecture measurements, both active and passive muscle–tendon forces and muscle fascicle length change can be determined (e.g. Arnold et al., 2010; Arnold and Delp, 2011). Such models may also be used in forward dynamics simulations to evaluate performance-based optimization criteria, which have provided considerable insight into the physiological bases of walking, running and jumping (e.g. Anderson and Pandy, 2001; Miller et al., 2012; Pandy et al., 1990; Umberger, 2010). Understanding how muscular, skeletal and neural traits interact to influence locomotor performance is an important goal not only for improving human health, but also for gaining new insights into the evolution of human locomotor behavior. Despite the considerable value of musculoskeletal modeling and simulation, no comparable model exists for any of our living, great ape relatives. Such a model is essential for providing an evolutionary context for human performance studies.

The common chimpanzee is both a facultative biped and our closest living relative (Goodman, 1999; Mikkelsen et al., 2005). As such, chimpanzees have long been used to gain insight into the origins and evolution of bipedal locomotion in humans (e.g. Elftman and Manter, 1935a; Elftman, 1944; Jenkins, 1972; Sockol et al., 2007; Stern and Susman, 1981; Taylor and Rowntree, 1973; Tardieu, 1992). The similarities and differences that exist in locomotor mechanics and energetics between chimpanzees and humans have provided a number of important insights into our physiological and anatomical evolution (see Aiello and Dean, 1990; Schmitt, 2003; Stern, 2000). For example, chimpanzees use approximately 75% more energy per distance walked than do humans (Rodman and McHenry, 1980; Sockol et al., 2007), suggesting that an important element in human locomotor evolution was reducing locomotor costs relative to our ape-like common ancestor. Musculoskeletal modeling permits decomposition of the mechanical and metabolic costs of a movement task among individual muscle–tendon units (Neptune et al., 2009; Umberger and Rubenson, 2011), and can provide insight into how these costs are influenced by the differences in skeletal structure, muscle properties and neural control between species.

Previous laboratory-based experimental measurements have included ground forces, joint movements and muscle activation patterns of common chimpanzees during bipedal walking (e.g. Ishida et al., 1985; Jenkins, 1972; Jungers et al., 1993; Kimura, 1996; Kumakura, 1989; Sockol et al., 2007; Stern and Larson, 1993; Stern

and Susman, 1981; Tardieu, 1992; Thorpe et al., 2004; Tuttle et al., 1979). These data have been important for addressing a number of specific issues related to the evolution of human locomotion; however, these data have generally been considered in isolation and can be quite difficult to integrate. Yet, this is a necessary step for understanding how the neuromusculoskeletal system produces locomotor movements (Zajac et al., 2002). A comprehensive model that permits simultaneous integration of kinematic, kinetic and muscular aspects of locomotion would substantially facilitate this task.

Here, we describe a 3D musculoskeletal model of the chimpanzee pelvis and hind limb. The model provides accurate representations of muscle moment arms and muscle–tendon lengths within the defined joint ranges of motion, and allows detailed examination of 3D moment-generating capabilities about the hip, knee, ankle, first tarsometatarsal and second–fifth metatarsophalangeal joints. It also permits the calculation of individual muscle–tendon unit force and moment-generating capabilities, which are subjected to a detailed sensitivity analysis. In addition, we compared predictions from the chimpanzee model with similar results obtained from human modeling and experimental studies to gain insights into the functional consequences of the morphological differences between the two species. A user-extensible version of this model will be made available at www.simtk.org, which can be viewed, manipulated and analyzed using the freely available biomechanical simulation software OpenSim (Delp et al., 2007).

MATERIALS AND METHODS

Model construction

Skeletal elements

The disarticulated skeleton of a 55 kg wild-shot adult male chimpanzee [*Pan troglodytes* (Blumenbach 1775)] housed at the American Museum of Natural History was used to reconstruct the 3D pelvis and hind limb model. The pelvis (innominates and sacrum) as well as the femur, patella, tibia, fibula, tarsals, metatarsals and phalanges of the right limb were CT scanned using a GE Lightspeed CVT scanner (GE Healthcare, Waukesha, WI, USA). Serial scans of each bone were collected at a slice thickness of 0.625–1.0 mm (voltage: 120 kV; current 70 mA). The CT scanner output a stack of DICOM image files for each bone, and these were imported into Avizo (Visualization Sciences Group, Burlington, MA, USA) for 3D reconstruction. The initial wire-frame renderings of each element were typically quite large. Therefore, the number of points and triangle polygons representing each element were down-sampled to a more manageable size (range: 1000 points for patella to 12,000 points for femur), without a noticeable loss of quality in the depiction of surface geometry. A final, watertight shell (i.e. a closed polygonal mesh surface) of the reconstructed element was created in Geomagic (Geomagic Engineering, Morrisville, NC, USA) for export into Software for Interactive Musculoskeletal Modeling (SIMM; Musculographics, Santa Rosa, CA, USA).

The skeletal elements were associated with six corresponding body segments defined in SIMM. These include, the pelvis, thigh, shank, hind and mid foot, hallux (first digit) and toes (second–fifth digits). Mobile articulations were assigned at the hip, knee, ankle, first tarsometatarsal, and second to fifth metatarsophalangeal joints by defining joint centers and rotational axes. The hip joint was modeled as a spherical articulation between the pelvis and femur. The center of the hip joint was found by fitting spheres to the acetabulum and the head of the femur, and then making the centers of the two spheres coincident. The knee joint had one rotational degree of freedom, which was coupled to translation of the tibia relative to the femur and translation and rotation of the patella relative to the tibia. The center of the knee was taken as the midpoint of a line between the medial and lateral femoral epicondyles. The profile of the chimpanzee femoral condyles has been described as being more circular than in humans (e.g. Heiple and Lovejoy, 1971; Tardieu, 1983); however, modeling the tibiofemoral articulation as a revolute joint led to considerable interpenetration of the tibia and femur. This problem was overcome by introducing translation in the joint that allowed the tibial plateau to track along the contours of the femoral condyles without any bony penetration. The patella was similarly allowed to translate and rotate as a function of the knee flexion angle, such that the patella tracked along the contours of the femoral condyles. The talocrural joint was modeled as a revolute joint between the tibia–fibula and talus, with the rotational axis running between the inferior aspects of the medial and lateral malleoli (Elftman and Manter, 1935b; Latimer et al., 1987). The first tarsometatarsal joint and the metatarsophalangeal joints of the second through fifth digits were also modeled as revolute joints, with the axes determined from congruence of the adjoining skeletal elements.

In order to provide a reference position from which joint angles can be expressed, a neutral posture was defined where the positions of all joint angles were equal to zero. For the hip, the neutral position was set at full extension, with an intermediate position between abduction–adduction and internal–external rotation. The knee joint was also fully extended in the neutral position. The ankle and metatarsophalangeal joints were set between dorsiflexion and plantar flexion, while the tarsometatarsal joint was positioned between abduction and adduction. In the neutral posture, the pelvis and femur were aligned with the vertical. The chimpanzee tibia has a substantial curvature in both the sagittal and frontal planes; thus, the tibia was aligned in its reference frame so as to maximize congruence between the femoral condyles and the tibial plateau. The foot bones were oriented in their respective reference frames following Elftman and Manter (Elftman and Manter, 1935b). The range of motion limits at each of the joints was set based on cadaveric studies (Holowka and O'Neill, in press; Nagano, 2001; Payne et al., 2006; Thorpe et al., 1999). These limits are reported in Table 1.

Muscle–tendon units

A total of 35 muscle–tendon units from the pelvis and right hind limb were represented in the model using 44 muscle–tendon paths (Fig. 1). This includes all of the flexors–extensors, abductors–adductors and mediolateral rotators capable of significant

Table 1. Model joint ranges of motion (deg)

	Hip	Hip	Hip	Knee	Ankle	Tarso-metatarsal (digit 1)	Metatarso-phalangeal (digits 2–5)
	Flexion–extension	Abduction–adduction	Internal–external rotation	Flexion–extension	Flexion–extension	Abduction–adduction	Flexion–extension
Maximum	120 (flexed)	10 (adducted)	20 (internal)	0 (neutral)	50 (dorsiflexed)	25 (abducted)	30 (flexed)
Minimum	0 (neutral)	−50 (abducted)	−40 (external)	−140 (flexed)	−60 (plantarflexed)	−30 (adducted)	−50 (extended)

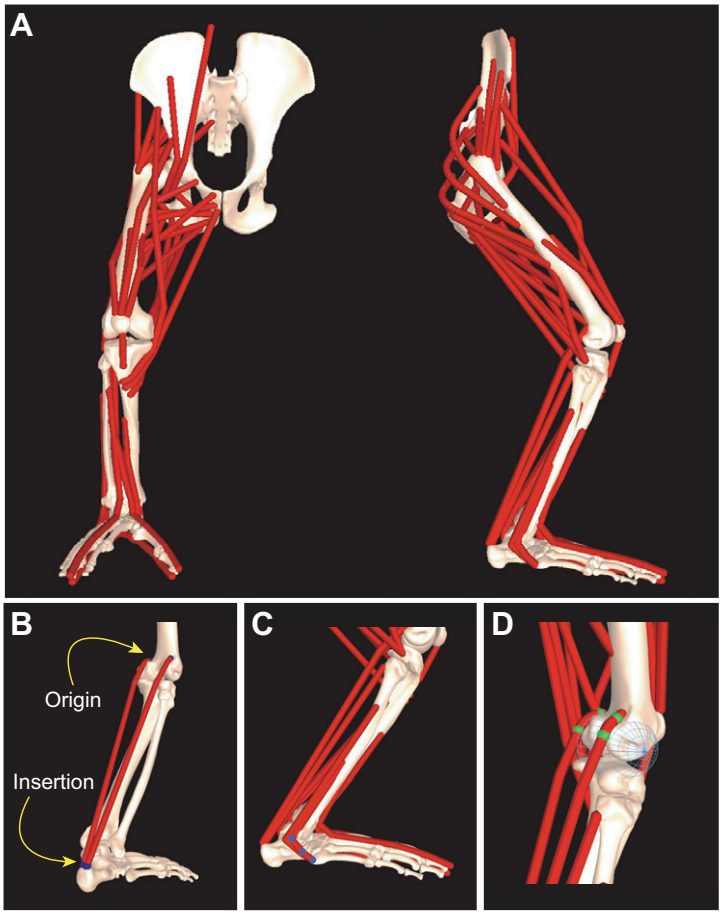

Fig. 1. Three-dimensional musculoskeletal model of the chimpanzee pelvis and hind limb. (A) The skeletal elements include the pelvis (innominates and sacrum), femur, patella, tibia, fibula, tarsals, metatarsals and phalanges, with mobile articulations at the hip, knee, ankle, first tarsometatarsal, and second–fifth metatarsalphalangeal joints. Thirty-five muscle–tendon units are represented using 44 muscle–tendon paths. (B) The muscle–tendon units used one or more line segment paths that were assigned origin and insertion points based on skeletal landmarks, published muscle maps and cadaveric dissection. (C) Via points and (D) wrapping surfaces were used to constrain muscle–tendon units to realistic paths.

force production during movement. A list of these anatomical muscle–tendon units and the muscle–tendon paths used to represent them in the model, is given in Table 2.

Each muscle–tendon path was assigned origin and insertion points based on a combination of skeletal landmarks, published muscle maps (Swindler and Wood, 1982; Uhlmann, 1968; Stern, 1972) and cadaveric dissections (Fig. 1A,B). The muscle–tendon path origin and insertion were positioned as near as possible to the centroid of the muscle attachment area. Some muscles with broad attachments, such as the mm. gluteals and m. adductor magnus, were not well represented using a single muscle–tendon path. In these cases, three or four separate muscle–tendon paths were used to represent the full distribution of the muscle–tendon unit. Using multiple muscle–tendon paths to represent a single muscle–tendon unit is a common modeling practice (e.g. Arnold et al., 2010; Delp et al., 1990; Van der Helm et al., 1992), and is consistent with electromyographic measurements indicating that chimpanzees recruit isolated subunits of some large hind limb muscles during movement (Stern and Susman, 1981). In one case, three small external (lateral) rotators of the hip (m. superior gemellus, m. inferior gemellus and m. obturator internus) were judged to have such similar paths as to be adequately represented by a single muscle–tendon unit. The small, intrinsic muscles of the foot were not included in the current model; however, the extensible nature of our model permits their addition for future studies addressing issues specific to intrinsic foot function in chimpanzees.

Muscle–tendon units were constrained to anatomically realistic paths using a combination of via points (Fig. 1C) and wrapping surfaces (i.e. cylinders and ellipsoids; Fig. 1D). These parameters place boundary conditions on the movement of specific points or components of muscle–tendon paths (Delp et al., 1990; Delp and Loan, 2000; Van der Helm et al., 1992). *In vivo*, these constraints are present because of bone, retinacula or other muscle–tendon units.

Hill muscle models

The force-generation capability of each muscle–tendon unit was represented using a generic Hill-type muscle model (Delp et al., 1990; Zajac, 1989). The Hill muscle model consists of a contractile element arranged in parallel with one elastic element, which are both in series with another elastic element (Fig. 2A). While the contractile and parallel elastic elements are generally associated with the properties of the muscle fibers, and the series elastic element is commonly equated to the tendon, it is important to note that these are both modeling approximations. In particular, it is important to be clear that the ‘tendon’ in the muscle model represents the effects of all in-series elasticity in a muscle, including that due to the aponeurosis or to sarcomeric proteins. Thus, even muscles with little or no external tendon, such as the chimpanzee m. gluteus medius or m. adductor magnus, will have non-zero tendon lengths in the muscle model. Given this, a generic Hill model was scaled to characterize specific muscle–tendon units by specifying the values of four parameters: maximum isometric force, optimal fiber length, tendon slack length and pennation angle. In order to minimize confusion, the term fascicle length is used to refer to data derived from experimental anatomical measurement, while fiber length is used to refer to the related muscle model variable. To determine the values of the muscle

Table 2. Muscle model parameter values

Muscle	Abbreviation	Mass[a] (kg)	Optimal fiber length[a] (m)	Pennation angle[c] (deg)	PCSA[e] (m^2)	Peak isometric force[f] (N)	Tendon slack length[g] (m)	Tendon length/ fiber length[h]
Gluteus maximus								
Gluteus maximus proprius cranial	glmax1	0.053	0.129	7	0.00039	122.9	0.084	0.65
Gluteus maximus proprius middle	glmax2	0.046	0.114	7	0.00039	122.9	0.116	1.02
Gluteus maximus proprius caudal	glmax3	0.042	0.102	7	0.00039	122.9	0.109	1.07
Gluteus maximus ischiofemoralis	glmax4	0.305	0.107	7	0.00270	850.5	0.081	0.76
Gluteus medius								
Gluteus medius lateral	glmed1	0.128	0.095	0	0.00127	400.1	0.031	0.33
Gluteus medius middle	glmed2	0.159	0.118	0	0.00127	400.1	0.046	0.39
Gluteus medius medial	glmed3	0.112	0.083	0	0.00127	400.1	0.025	0.30
Gluteus minimus								
Gluteus minimus lateral	glmin1	0.040	0.086	0	0.00044	138.6	0.015	0.17
Gluteus minimus middle	glmin2	0.033	0.071	0	0.00044	138.6	0.012	0.17
Gluteus minimus medial	glmin3	0.029	0.063	0	0.00044	138.6	0.013	0.21
Adductor magnus[b]								
Adductor magnus proximal	admag1	0.037	0.080	0	0.00044	139.0	0.035	0.44
Adductor magnus middle	admag2	0.051	0.110	0	0.00044	139.0	0.049	0.45
Adductor magnus distal	admag3	0.066	0.141	0	0.00044	139.0	0.066	0.47
Adductor magnus ischial	admag4	0.074	0.159	0	0.00044	139.0	0.083	0.52
Adductor longus[b]	adlong	0.063	0.088	0	0.00068	214.2	0.078	0.89
Adductor brevis[b]	adbrev	0.155	0.112	0	0.00131	412.7	0.025	0.22
Iliopsoas[b]								
Iliacus	iliacus	0.097	0.106	16	0.00086	270.9	0.086	0.81
Psoas (major and minor)	psoas	0.213	0.088	20	0.00228	718.2	0.190	2.16
Quadratus femoris	quadfem	0.013	0.044	0	0.00028	88.2	0.011	0.25
Gemelli[d,i]	gem	0.048	0.043	0	0.00105	330.8	0.020	0.47
Piriformis	piri	0.027	0.068	0	0.00037	116.6	0.045	0.66
Pectineus[d]	pect	0.054	0.120	0	0.00042	132.3	0.007	0.06
Obturator externus[d]	obex	0.074	0.078	0	0.00090	283.5	0.025	0.32
Semimembranosus	semimem	0.100	0.180	0	0.00052	163.8	0.117	0.65
Semitendinosus	semiten	0.149	0.297	0	0.00047	148.1	0.105	0.35
Biceps femoris, long head	bflh	0.126	0.179	10	0.00066	207.9	0.127	0.71
Biceps femoris, short head	bfsh	0.073	0.114	5	0.00060	189.0	0.025	0.22
Gracilis	grac	0.178	0.257	0	0.00065	204.8	0.090	0.35
Sartorius[d]	sart	0.086	0.342	0	0.00024	75.6	0.103	0.30
Rectus femoris	recfem	0.138	0.089	15	0.00146	459.9	0.213	2.39
Vastus intermedius	vasint	0.198	0.103	15	0.00181	570.2	0.051	0.50
Vastus lateralis	vaslat	0.327	0.114	21	0.00271	853.7	0.056	0.49
Vastus medialis	vasmed	0.152	0.110	20	0.00130	409.5	0.055	0.50
Gastrocnemius lateralis	gaslat	0.100	0.091	13	0.00104	327.6	0.203	2.23
Gastrocnemius medialis	gasmed	0.134	0.091	30	0.00139	437.9	0.225	2.47
Soleus	sol	0.190	0.063	23	0.00285	897.8	0.167	2.65
Tibialis anterior[b]	tibant	0.121	0.104	11	0.00110	346.5	0.086	0.83
Tibialis posterior	tibpos	0.097	0.029	26	0.00316	995.4	0.161	5.55
Flexor digitorum tibialis	fdt	0.061	0.060	16	0.00096	302.4	0.305	5.08
Flexor digitorum fibularis	fdf	0.120	0.073	16	0.00155	488.3	0.246	3.37
Peroneous (fibularis) brevis	perbrev	0.036	0.068	16	0.00050	157.5	0.070	1.03
Peroneous (fibularis) longus	perlong	0.074	0.057	18	0.00123	387.5	0.208	3.65
Extensor hallucis longus[d]	ehl	0.018	0.120	0	0.00014	44.1	0.142	1.18
Extensor digitorum longus[d]	edl	0.043	0.160	0	0.00025	78.8	0.174	1.09

[a]Muscle masses and optimal fiber lengths were scaled based on body mass from Thorpe et al. (Thorpe et al., 1999), except where specifically indicated.
[b]Muscle masses and optimal fiber lengths for adductor, iliopsoas and tibialis anterior muscles were scaled based on body mass from Nagano (Nagano, 2001).
[c]Pennation angles were based on Nagano (Nagano, 2001).
[d]Muscles for which no pennation angles were available were assigned a value of 0 deg.
[e]Physiological cross-sectional area (PCSA) values were calculated from muscle mass, optimal fiber length and muscle density (1059.7 kg m^{-3}).
[f]Peak isometric forces were calculated from PCSA based upon a specific tension of 315,000 N m^{-2}.
[g]Tendon slack lengths were determined using a numerical optimization procedure (Manal and Buchanan, 2004).
[h]Data in this column represent the ratio of tendon slack length to optimal fiber length.
[i]The 'gemelli' actuator combined the properties of the m. superior gemellus, m. inferior gemellus and m. obturator internus.

model parameters, we combined published measurements with geometric scaling and numerical optimization.

The maximum isometric force was calculated from the physiological cross-sectional area (PCSA; m^2) and specific tension (N m^{-2}) for skeletal muscle. To determine muscle PCSA values for the chimpanzee model, we used muscle mass, fascicle length and pennation angle data from cadaveric dissections of fresh-frozen male chimpanzee specimens [one 6 year old (Thorpe et al., 1999) and one 7 year old (Nagano, 2001)]. The use of young specimens helped mitigate the known underestimation of PCSA in some adult or elderly animals because of age-related muscle atrophy (e.g. Narici et al., 2003).

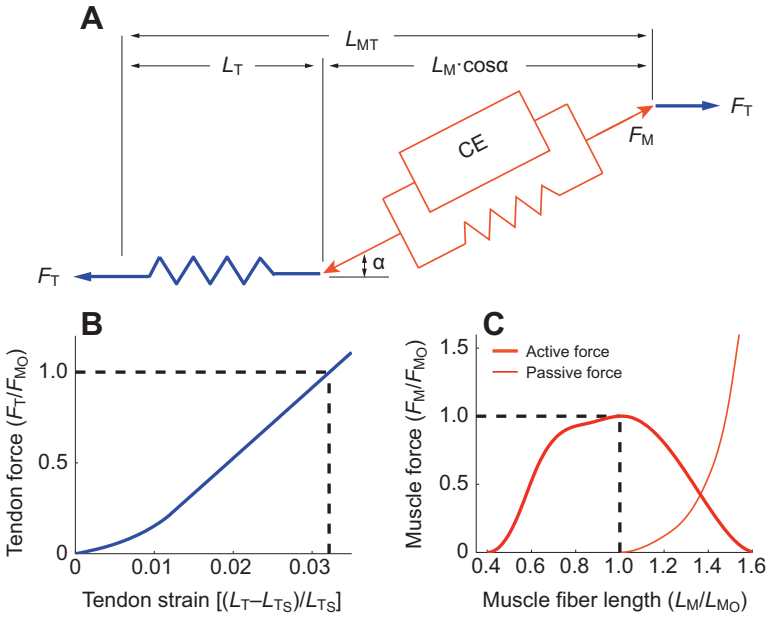

Fig. 2. Hill-type muscle model used to estimate forces as a function of musculotendon length and activation. (A) The muscle model consists of a contractile element (CE) arranged in parallel with an elastic element, which primarily represent the mechanical properties of the muscle fibers. Both of these elements are in series with another elastic element, which primarily represent the mechanical properties of the tendon. (B) Tendon force depends nonlinearly on tendon length and is related to muscle force according to: $F_T=F_M \cos\alpha$, where F_T is tendon force, F_M is muscle force and α is pennation angle. (C) Isometric muscle force is taken to be equal to the sum of passive force and active force, both of which depend nonlinearly on muscle length. Muscle length and tendon length are related to total musculotendon length according to: $L_{MT}=L_T+L_M \cos\alpha$, where L_{MT} is musculotendon length, L_T is tendon length and L_M is muscle length. L_{MO}, optimal muscle length; L_{TS}, tendon slack length; F_{MO}, peak isometric muscle force. Adapted from Delp et al. (Delp et al., 1990).

In order to maintain proportionality among different hind limb muscles, we preferred to base our muscle mass and fascicle length values on the near-complete data set of Thorpe et al. (Thorpe et al., 1999). However, for the m. iliacus, the mm. psoas (major and minor), the mm. adductors (adductor magnus, longus and brevis) and the m. tibialis anterior, muscle masses and fascicle lengths were drawn from Nagano (Nagano, 2001). This was a necessary step, as Thorpe et al. (Thorpe et al., 1999) did not report data for the mm. iliopsoas, and their adductor fascicle lengths were typically longer than the total muscle–tendon unit lengths in our model. In addition, the dorsiflexor-to-plantar flexor PCSA ratio in Thorpe et al. (Thorpe et al., 1999) was quite low compared with other chimpanzee data (Holowka and O'Neill, in press). Using the Nagano (Nagano, 2001) data for the m. tibialis anterior yielded a muscle fiber length similar to that in the Thorpe et al. (Thorpe et al., 1999) data set, with less of an imbalance between dorsiflexion and plantar flexion strength. Nagano (Nagano, 2001) did not report raw muscle masses and fascicle lengths; however, these values could be recovered by reversing the scaling procedures performed on his data. Pennation angles were also not reported in Thorpe et al. (Thorpe et al., 1999), and therefore were taken from Nagano (Nagano, 2001) as well. For six muscles, pennation angles were unavailable from any source, and as a result those angles were set at zero (Table 2).

The nominal muscle mass (M_m) and fascicle length (L_f) data were scaled to account for the larger body mass of the specimen that our model was based on (55 kg), relative to the specimens in Thorpe et al. [37 kg (Thorpe et al., 1999)] and Nagano [32 kg (Nagano, 2001)] from which the muscle architecture data were derived. Assuming geometric similarity among common chimpanzees, skeletal muscle mass was scaled to body mass (M_b) as $M_b^{1.0}$, and fascicle length was scaled to $M_b^{0.33}$. Combining the scaled muscle masses and fascicle lengths, the PCSA of each muscle was calculated as:

$$PCSA = \frac{M_m}{L_f \cdot \rho}, \quad (1)$$

where ρ is the density of skeletal muscle (1059.7 kg m^{-3}) (Mendez and Keys, 1960). The effects of pennation angle (α) on force-producing capacity were taken into account when equilibrating muscle and tendon forces (Fig. 2A).

For muscle–tendon units that were represented using multiple muscle–tendon paths, the total PCSA was equally divided among the individual paths. The muscle–tendon path for the mm. gluteus maximus was an exception to this approach, as its superior component (m. gluteus maximus proprius) is substantially smaller than its inferior component (m. gluteus maximus ischiofemoralis) (Stern, 1972). In this case, the m. gluteus maximus ischiofemoralis was assigned 70% of the total PCSA, while the three muscle–tendon paths representing the m. gluteus maximus proprius split the remaining 30%. PCSA represents the total cross-section of muscle available for producing force (m^2), which together with specific tension (N m^{-2}) determines the force-generating capacity of muscle. The specific tension of vertebrate skeletal muscle is typically reported to be 150,000–300,000 N m^{-2} (Josephson, 1993). While the force–length and force–velocity properties of chimpanzee muscles are unknown, at least one recent study has proposed that chimpanzees have larger than average muscle force-producing capabilities (Scholz et al., 2006). Therefore, in the absence of direct measurements, an estimate of specific tension (315,000 N m^{-2}) that is slightly above these values, but within the measured range for mammalian skeletal muscle (cf. Brown et al., 1998), was used. This value is similar, but still a bit higher than measurements from other primates, including humans (Maganaris et al., 2001) and macaques (Fitts et al., 1998). The maximum isometric force for each muscle model was obtained by multiplying the scaled PCSA values by the estimated specific tension.

The optimal fiber length for each modeled pelvis and hind limb muscle was taken to be equivalent to its scaled fascicle length. Combining our optimal fiber lengths and the muscle–tendon unit lengths from the musculoskeletal model, we estimated the tendon slack length for each muscle using a numerical optimization procedure (Manal and Buchanan, 2004). In implementing the tendon slack length optimization, the restrictions in the original algorithm that muscle fibers only operate on the ascending limb of the active force–length curve and tendons only function on the linear portion of their stress–strain curve were removed. Optimizations were performed using the constrained nonlinear optimization function (fmincon) in the MATLAB Optimization Toolbox (The MathWorks, Natick, MA, USA).

Methods

Moment arms

As an initial evaluation of the robustness of the model, predicted flexion–extension moment arms for hip, knee and ankle muscles were compared with values derived from experiments performed on cadaveric chimpanzee specimens (Holowka and O'Neill, in press; Payne et al., 2006; Thorpe et al., 1999). The femur, tibia and foot lengths of Thorpe et al. (Thorpe et al., 1999), Payne et al. (Payne et al., 2006) and Holowka and O'Neill (Holowka and O'Neill, in press) are, coincidentally, quite similar to the model. As such, the use of limb segment lengths to scale the muscle moment arms had no significant impact on their relative magnitudes. Thus, for ease of comparison, the model (predicted) and chimp (observed) muscle moment arms are presented in dimensional form.

Maximum isometric joint moments

The model can also be used to estimate the moment-producing capability of an individual muscle–tendon unit at a given 3D joint position, by calculating its moment arm length and tendon force. Tendon force is equal to the sum of the active muscle fiber force and the passive force of the parallel elastic element, multiplied by the cosine of the pennation angle. Active (isometric) force generation depends on the muscle force–length curve and muscle activation, which can range from 0 (no activation) to 1 (full activation). In passive force generation, muscle fibers are stretched past their optimal length on the force–length curve and force is developed in the parallel elastic element. In order to calculate maximum isometric joint moments, individual muscles were fully activated and forces were computed at lengths corresponding to the full joint range of motion. Each model joint was positioned in its approximate standing or 'mid-stance' posture (following Jenkins, 1972) while the hip, knee and ankle were moved through their full joint ranges of motion.

Sensitivity analysis

In developing the model, several decisions about its structure were made and numerous model parameters were specified. Given this, understanding the sensitivity of model outputs to variations in the model structure and parameter values is essential. To this end, the sensitivity of muscle–tendon moment arms and maximum isometric joint moments to variations in muscle path parameters and muscle architecture parameters were evaluated.

The muscle–tendon paths in the model are specified by origin and insertion points, and in many cases include via points and wrapping surfaces. The effects of uncertainty in these parameters on the resulting musculoskeletal geometry were demonstrated in three muscles, the m. gluteus medius (middle part), the m. vastus intermedius and the m. soleus, which reflect a range of complexity in pathway specification. For these muscles, muscle–tendon path parameters were varied individually, and the effects of those changes on the magnitudes of the moment arms were evaluated. For the m. gluteus medius, the origin was moved 1 cm cranially and caudally along the ilium and the insertion was moved 1 cm cranio-medially and caudo-laterally along the contour of the proximal femur. The wrapping surface that prevents the m. gluteus medius from penetrating the ilium with the hip abducted and internally (medially) rotated was also removed. For the m. vastus intermedius, the via point between the origin and the patellar attachment was moved 1 cm proximally and distally along the femur. Also, the wrapping cylinder that prevents penetration through the distal femur with knee flexion was changed in diameter by ±10%. The kinematic function that prescribed how the patella tracked along the contour of the femoral condyles was changed in magnitude by ±10%. This change had the effect of displacing the line of action of the m. vastus intermedius further away from (+10% change) or closer to (−10% change) the axis of rotation of the knee. For the m. soleus, the origin was moved 0.5 cm proximally and distally along the fibula, and the insertion was moved 0.5 cm anteriorly and posteriorly along the calcaneus. Smaller perturbations were used for the m. soleus than for the more proximal muscles to prevent unrealistic situations, such as a muscle attachment being far removed from the corresponding skeletal element. The anatomically realistic ankle joint axis, running between the malleoli, was also replaced with a pure mediolateral axis through the center of the ankle joint.

The maximum isometric moments generated about the joints are a function not only of musculoskeletal geometry, but also of the force-generating capacities of the muscle. The peak isometric forces generated by the muscle, in turn, depend on the muscle model parameter values. To evaluate the effects of uncertainty in muscle model parameter values, we varied maximum isometric force, optimal fiber length, pennation angle and tendon slack length, and assessed the effects on the maximum isometric moments. For each individual model parameter, we varied the nominal values by ±5% and ±10%, while holding all other model parameters constant. We then recalculated the maximal isometric joint moment over the full range of joint motion. Results are presented for several muscles (m. gracilis, m. sartorius, m. adductor magnus proximal, m. psoas, m. rectus femoris, m. vastus medialis, m. vastus intermedius, m. vastus laterialis, m. biceps femoris long head, m. biceps femoris short head, m. semimembranosus, m. gastrocnemius medialis, m. gastrocnemius lateralis and m. tibialis posterior) that demonstrate the range of sensitivities to muscle model parameter values.

Hip joint angle interactions

The skeletal model includes a spherical hip joint with relatively large ranges of motion about the three primary joint axes. Consequently, the moment arms of the hip muscles about specific joint axes will depend on the values of the joint angles about the other two axes (cf. Arnold and Delp, 2001). Of course, the degree of these cross-sensitivities may vary considerably among muscles. These effects were evaluated by computing the muscle moment arms about one of the hip joint axes, while systematically varying the angles of the other two joint axes for all of the muscles crossing the hip. Results are presented for four muscles [m. gluteus maximus proprius (caudal part), m. gluteus minimus (middle part), m. pectineus and m. adductor longus] that demonstrate the range of these cross-sensitivities.

Chimpanzee versus human muscle architecture

Following the validation and sensitivity analyses, we compared muscle PCSA, fiber length and mass data from the chimpanzee model with corresponding data from a similar human musculoskeletal model (Arnold et al., 2010). Both of these models are based on the best available muscle architecture data for each species, except that the data underlying the human model are presently more extensive than for the chimpanzee model.

RESULTS

Moment arms

The moment arms predicted by the model were generally in good agreement with the moment arm functions from tendon-excursion experiments. That is, for a given muscle–tendon unit, the model predicted a similar magnitude and direction over the measured joint flexion–extension range.

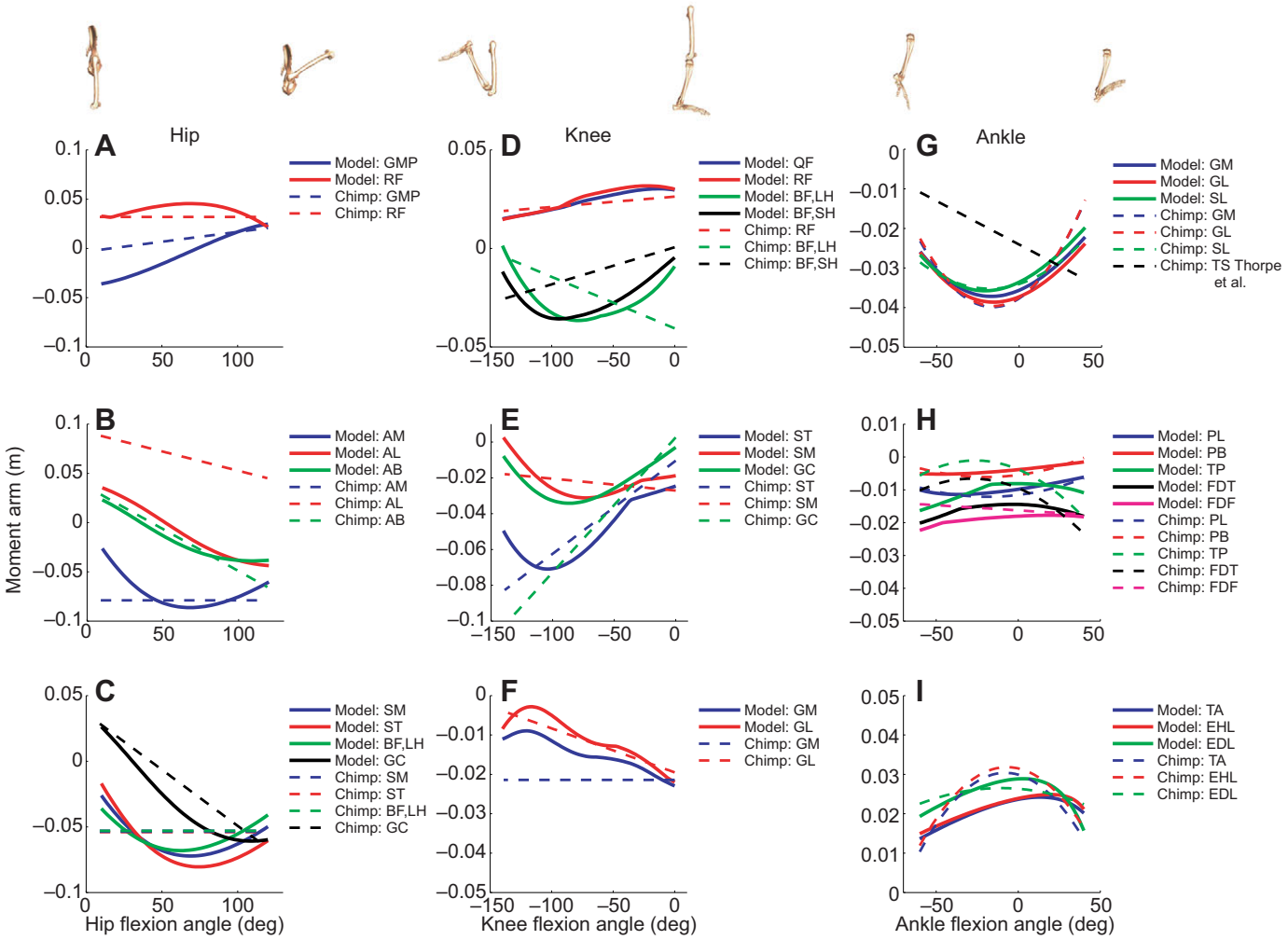

Fig. 3. Moment arms of muscles and muscle–tendon units crossing the (A–C) hip, (D–F) knee and (G–I) ankle predicted from the chimpanzee musculoskeletal model ('Model') and compared with measurements from cadaveric tendon-excursion experiments ('Chimp'). Model predictions are solid lines, while cadaveric tendon-excursion measurements are dashed lines. The same colors indicate corresponding muscle–tendon units in the 'Model' and 'Chimp'. The tendon-excursion measurements are taken from Thorpe et al. (Thorpe et al., 1999), Payne et al. (Payne et al., 2006) and Holowka and O'Neill (Holowka and O'Neill, in press). The muscle–tendon unit names are abbreviated as: GMP, gluteus maximus proprius; RF, rectus femoris; AM, adductor magnus; AL, adductor longus; AB, adductor brevis; SM, semimebranosus; ST, semitendinosus; BF,LH, biceps femoris, long head; GC, gracilis; QF, quadriceps muscles; BF,SH, biceps femoris, short head; GM, gastrocnemius medialis; GL, gastrocnemius lateralis; SL, soleus; PL, peroneus longus; PB, peroneus brevis; TP, tibialis posterior; FDT, flexor digitorum tibialis; FDF, flexor digitorum fibularis; TA, tibialis anterior; EHL, extensor hallicus longus; and EDL, extensor digitorum longus. 'TS Thorpe et al.' shows the moment arm given in Thorpe et al. (Thorpe et al., 1999) for the triceps surae (i.e. GM, GL and SL) muscles as a group.

At the hip (Table 1, Fig. 3A–C), the tendon-excursion data for the m. gluteus maximus in *P. troglodytes* is limited to a single measurement, given in Payne et al. (Payne et al., 2006). The model prediction for the m. gluteus maximus proprius (cranial part) was similar to this measurement in direction, but with a larger extensor moment arm maintained through the first two-thirds of hip flexion. Moment arms for the ischial path of the m. adductor magnus and for the m. adductor brevis are both similar in direction and magnitude to the *P. troglodytes* tendon-excursion data in Thorpe et al. (Thorpe et al., 1999), while the model m. adductor longus is smaller, and exhibits an extensor moment arm for most of hip flexion. The model hamstrings (m. semimembranosus, m. semitendinosus and m. biceps femoris, long head) and remaining muscles around the hip (m. rectus femoris, m. gracilis) are all quite similar to the moment arm functions in Thorpe et al. (Thorpe et al., 1999), with the main difference being the presence of higher-order (i.e. nonlinear) phenomena in the model predictions.

For the knee (Table 1, Fig. 3D–F), the model predictions for the quadriceps muscles are quite similar in both direction and magnitude to the tendon-excursion measurements for the m. rectus femoris. Thorpe et al. (Thorpe et al., 1999) indicate that the moment arm function for rectus femoris – rather than their quadriceps muscle function – provides the best characterization of the mm. vasti (m. vastus lateralis, m. vastus intermedius and m. vastus medialis) and the m. rectus femoris as a group. The model hamstrings (m. semimembranosus, m. semitendinosus and m. biceps femoris, long head) are all similar in magnitude and direction to the moment arm functions in Thorpe et al. (Thorpe et al., 1999). The m. gracilis is similar in magnitude in the first half of knee flexion, but predicts a smaller moment arm in the second half of knee flexion than the tendon-excursion experiment

indicates. Finally, the model m. gastrocnemius lateralis is almost identical in magnitude and direction to that in Thorpe et al. (Thorpe et al., 1999), while the model m. gastrocnemius medialis predicts a decrease in moment arm magnitude with increasing knee flexion.

At the ankle (Table 1, Fig. 3G–I), the model predictions for the m. gastrocnemius medialis, m. gastrocnemius lateralis and m. soleus are similar in both magnitude and direction to the tendon-excursion measurements of Holowka and O'Neill (Holowka and O'Neill, in press). Thorpe et al. (Thorpe et al., 1999) provide a single linear function for these three muscles as a group, and their moment arm function is smaller in plantar flexion, but slightly larger in maximum dorsiflexion than the muscle-specific measurements of Holowka and O'Neill (Holowka and O'Neill, in press). The model predictions for the deep plantar flexors (m. flexor digitorum tibilais, m. flexor digitorum fibularis, m. tibialis posterior, m. peroneus longus and m. peroneus brevis) and dorsiflexors (m. extensor digitorum longus, m. extensor hallicus longus and m. tibialis anterior) are all quite close in direction and magnitude to the measurements of Holowka and O'Neill (Holowka and O'Neill, in press).

Maximum isometric joint moments

On average, the active hip moments are largest in the extensors and adductors, with the internal and external rotators having similar strength (Fig. 4A–C). In contrast, the passive moments generated by the hip muscle–tendon units are quite small throughout abduction–adduction and internal–external rotation, but increase from 5 to 40 N m in the hip extensors when the hip is positioned in 80 to 120 deg of flexion. At the knee, the active moment was approximately two times larger in the extensors than in the flexors, with the passive moment increasing in the quadriceps muscle–tendon units to a maximum of 4 N m at −140 deg of flexion (Fig. 4D). At the ankle, the active moment was more than six times larger in plantar flexion than dorsiflexion. The passive moment in the plantar flexors increased from 1 to 14 N m through the full range of dorsiflexion (Fig. 4E).

Sensitivity analysis

The effects of changing muscle path parameters on muscle moment arms varied considerably, both among muscles as well as among pathway parameters (Fig. 5). For the m. gluteus minimus (middle part), neither the flexion–extension nor the abduction moment arms were affected by varying the location of the origin. In contrast, varying the location of the insertion did alter the moment arms, especially with the hip joint flexed and abducted (Fig. 5A,B). The effects of varying the insertion location on the abduction moment arm were relatively straightforward, with a caudo-distal displacement increasing the moment arm and a cranio-medial displacement reducing the moment arm (Fig. 5B). The effects of varying the insertion location on the flexion–extension moment arm were more complex, depending heavily on the angle of hip flexion (Fig. 5A). The iliac wrapping function had almost no effect on the flexion–extension moment arm (Fig. 5A), but did alter the abduction moment arm if the hip was abducted more than 20 deg (Fig. 5B).

Changing the location of the via point between the m. vastus intermedius origin and the patellar attachment had little effect on the knee extension moment arm (Fig. 5C). The m. vastus intermedius engages a wrapping cylinder in the femoral condyles at ~80 deg of knee flexion. With the knee flexed more than 80 deg, the moment arm was affected by changes in the wrapping cylinder, but not by

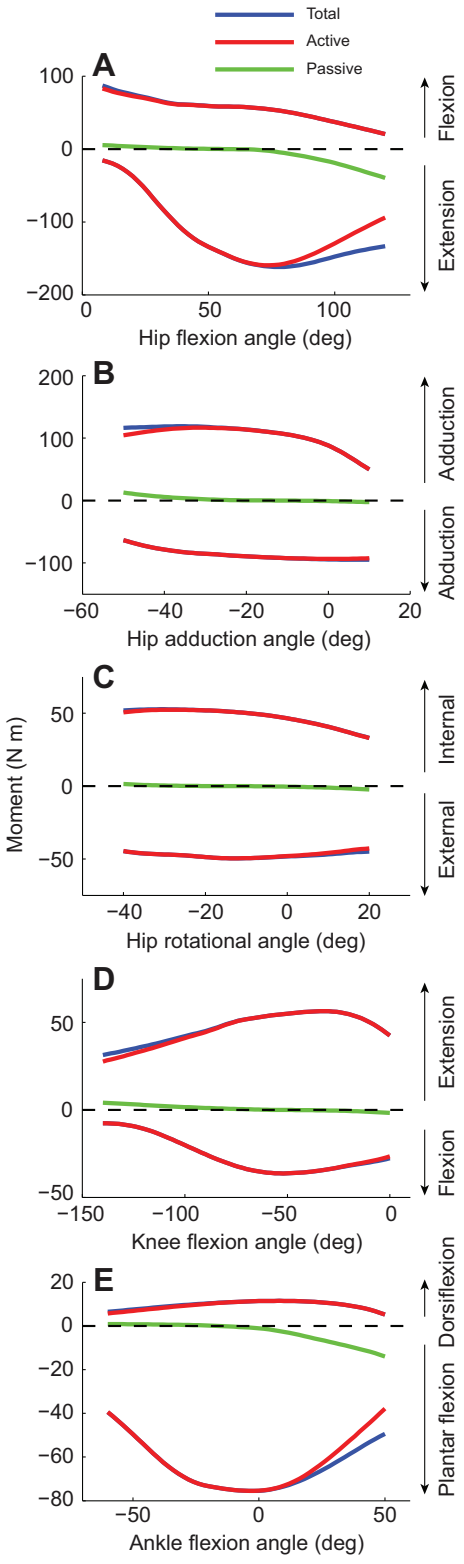

Fig. 4. Total, active and passive maximum isometric joint moments generated by muscles and muscle–tendon units crossing the hip, knee and ankle predicted from the chimpanzee musculoskeletal model. The approximate standing or 'mid-stance' posture joint positions were −10 deg pelvic tilt, 0 deg pelvic list, 0 deg pelvic rotation, 45 deg hip flexion, −10 deg hip adduction, 0 deg hip rotation, −45 deg knee flexion, 20 deg ankle dorsiflexion, 0 deg metatarsophalangeal flexion and 0 deg first tarsometatarsal abduction angles, following Jenkins (Jenkins, 1972).

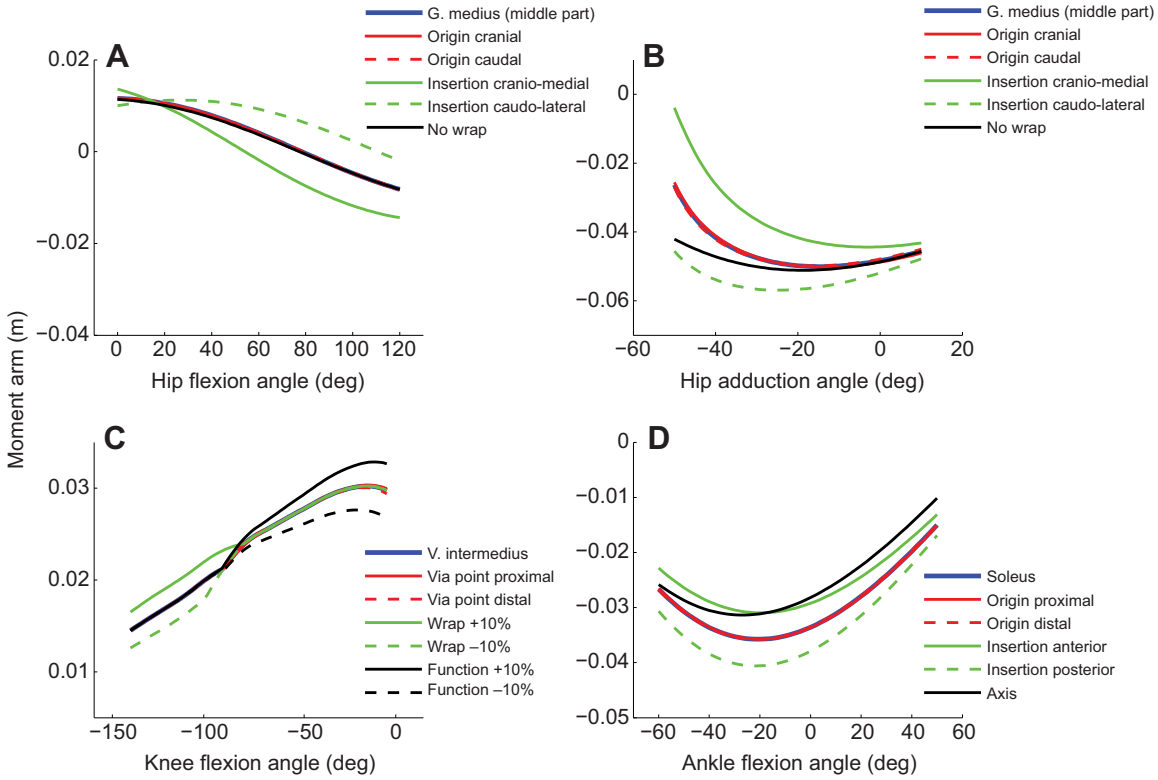

Fig. 5. Example sensitivity analysis results demonstrating the effects of uncertainty in muscle pathway parameters on muscle moment arms. In all panels, solid blue lines represent moment arms computed using the nominal model parameter values. (A,B) Red solid and dashed lines correspond to the m. gluteus medius (middle part) origin being moved cranially and caudally, respectively. Green solid and dashed lines correspond to the insertion being moved cranio-medially and caudo-laterally, respectively. The black solid line corresponds to the wrapping surface on the iliac crest being removed. (C) Red solid and dashed lines correspond to the via point between the m. vastus intermedius origin and the patellar insertion being moved proximally and distally, respectively. Green solid and dashed lines correspond to the radius of the wrapping cylinder at the femoral condyles being increased and decreased by 10%, respectively. Black solid and dashed lines correspond to the amplitude of the kinematic function defining patellar translation being increased and decreased by 10%, respectively. (D) Red solid and dashed lines correspond to the m. soleus origin being moved proximally and distally, respectively. Green solid and dashed lines correspond to the m. soleus insertion being moved anteriorly and posteriorly, respectively. The black solid line corresponds to the model's anatomically realistic ankle joint axis being replaced with a pure mediolateral axis. In all cases, the solid blue line underlies the solid red line almost completely.

altering the kinematic function describing patellar tracking along the femoral condyles (Fig. 5C). With the knee extended past 80 deg, the opposite was true. The same was generally true for all of the knee extensor muscles in the model.

Varying the location of the m. soleus origin had almost no effect on the plantar flexion moment arm (Fig. 5D). In contrast, moving the insertion had a relatively large effect on the plantar flexion moment arm, especially with the ankle plantar flexed around 10–30 deg. Predictably, moving the insertion posteriorly increased the magnitude of the moment arm, while moving the insertion anteriorly decreased the moment arm. The parameters describing the ankle joint axis of rotation also affected the m. soleus moment arm. When the anatomically realistic axis was replaced with a pure mediolateral axis, as would be the case in a two-dimensional model, the magnitude of the m. soleus moment arm was reduced (Fig. 5D).

The effects of varying muscle model parameters on the predicted isometric joint moments varied among muscles, and among muscle model parameters (Fig. 6). Peak isometric force had a direct, linear effect on the predicted joint moment (Fig. 6A). The effects of varying optimal fiber lengths were similar in magnitude to peak isometric force on average, but could be larger (e.g. m. vastus intermedius) or smaller (e.g. m. sartorius) in individual muscles (Fig. 6B). The effects of tendon slack length varied considerably across muscles, ranging from relatively small (e.g. m. biceps femoris, short head) to relatively large (e.g. m. rectus femoris), depending on the muscle in question (Fig. 6C). Pennation angle was the only muscle model parameter that had a uniformly small effect on the predicted joint moments (Fig. 6D).

The wide range of sensitivities to perturbing tendon slack lengths can be understood in part by considering the ratio of tendon slack length to optimal muscle fiber length (Table 2). For some muscles (e.g. m. tibialis posterior), tendon slack length is several times longer than optimal muscle fiber length, while the ratio for other muscles [e.g. m. adductor magnus (proximal part)] is well below 1.0, and in a few muscles (e.g. m. pectineus) the ratio is close to zero (Table 2). Muscles with a large ratio of tendon length to muscle fiber length, such as the m. tibialis posterior, tended to be more sensitive to changes in tendon slack length than muscles with a low ratio, such as the m. adductor magnus (proximal part) (Fig. 7). While these sensitivity measurements made at a single joint angle are useful for demonstrating the influence of muscle architecture on model performance, it is important to note that the degree of sensitivity actually may vary over the joint range of motion (cf. m. rectus femoris in Fig. 6C).

Also shown in Fig. 7 are the results obtained for the same muscles in the human musculoskeletal model of Arnold et al. (Arnold et al., 2010). For most hind limb muscles (all but eight),

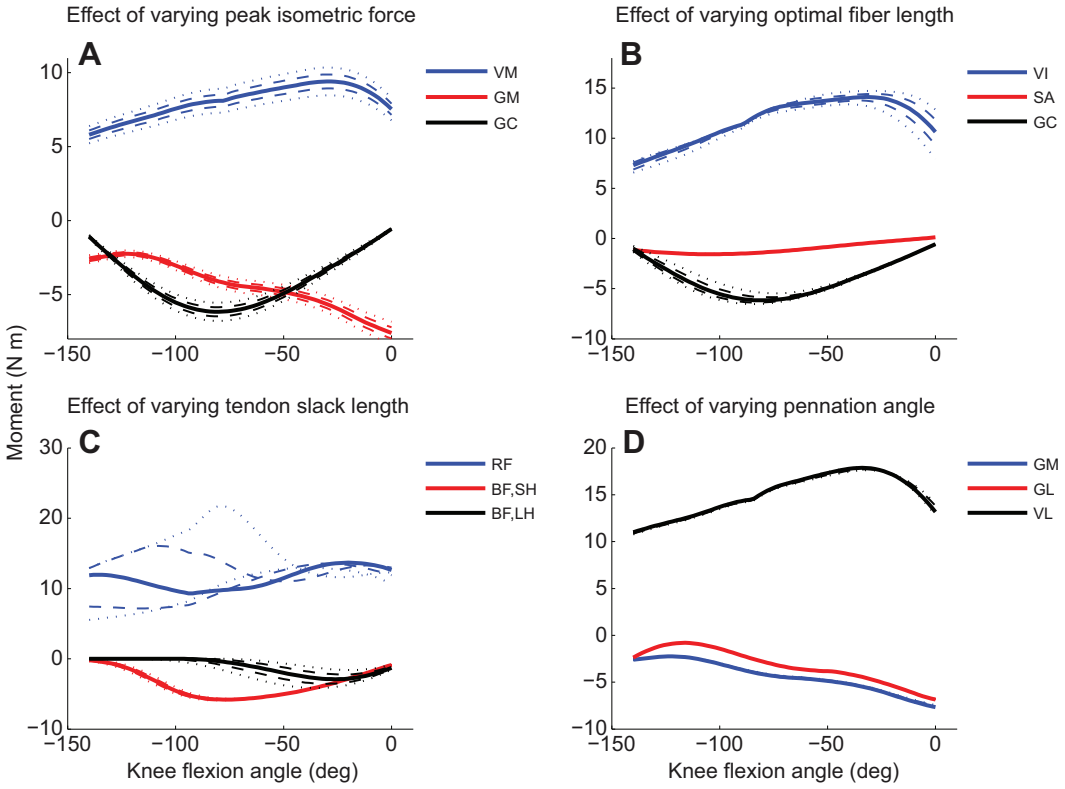

Fig. 6. Example sensitivity analysis results demonstrating the effects of uncertainty in muscle model parameter values on joint moments for selected muscles. Muscle model parameters included in the sensitivity analysis were: (A) peak isometric force, (B) optimal fiber length, (C) tendon slack length and (D) pennation angle. Solid lines represent joint moments generated using the nominal muscle parameter values defined in Table 2. Dashed and dotted lines represent joint moments generated when the muscle parameter values were perturbed ±5% and ±10%, respectively, from the nominal values. Results are shown for: (A) m. vastus medialis (VM), m. gastrocnemius medialis (GM) and m. gracilis (GC); (B) m. vastus intermedius (VI), m. sartorius (SA) and GC; (C), m. rectus femoris (RF), m. biceps femoris short head (BF,SH) and m. biceps femoris long head (BF,LH); and (D) GM, m. gastrocnemius lateralis (GL) and m. vastus lateralis (VL). Within each model parameter, muscles with blue lines represent examples of relatively large sensitivities, muscles with black lines represent examples of typical sensitivities and muscles with red lines represent examples of relatively low sensitivities.

the ratio of tendon slack length to muscle fiber length was greater in the human model than the chimpanzee model. Consequently, most of the muscles in the human model were more sensitive to changing tendon slack length. There were exceptions, such as the m. psoas (Fig. 7), where the tendon slack length to muscle fiber length ratio was greater in the chimpanzee model. However, in all of the cases where the ratio was greater in the chimpanzee model, those muscles had relatively low sensitivity to tendon slack length.

Hip joint angle interactions

The effects of changing one joint angle on the muscle moment arm about another joint axis differed among the hip muscles (Fig. 8). Varying the hip internal–external rotation angle had relatively little effect on the m. pectineus flexion–extension moment arm (Fig. 8B). In contrast, varying the hip adduction angle resulted in large changes in the m. gluteus maximus proprius (caudal part) extension moment arm (Fig. 8A). For the m. adductor longus, the flexion–extension moment arm switched sign approximately halfway through the adduction range of motion (Fig. 8C). However, the effect of changing the hip adduction angle was similar to that in the m. gluteus maximus proprius (caudal part), in that abducting the hip tended to decrease the magnitude of the m. adductor longus flexion–extension moment arm, regardless of the sign of the moment arm. There were also cases where changing one joint angle caused the moment arm about another joint axis to change sign. For example, externally rotating the hip, with the hip near full extension, caused the m. gluteus minimus (middle part) to change from a flexor to an extensor (Fig. 8D).

Chimpanzee *versus* human muscle architecture

The manner in which PCSA varies with mass and fiber length in the chimpanzee model was almost identical to that in the human model (Fig. 9A,B). That is, PCSA varies directly with muscle mass, with nearly the same slope for both species. The primary difference between species was the presence of two outliers in the human model, the m. gluteus maximus and the m. soleus (Fig. 9B). The m. gluteus maximus had a relatively small PCSA for its mass, while the m. soleus had an especially large PCSA for its mass. PCSA does not vary directly with fiber length for either species (Fig. 9C,D). In muscles with short fibers, PCSA is relatively independent of fiber length, while muscles with long fibers always have small PCSAs. The main difference between species was the presence of more extreme architectures in humans (Fig. 9D), including cases of both large PCSA with short fibers (m. soleus) and small PCSA with long fibers (m. sartorius).

DISCUSSION

Herein, a 3D musculoskeletal model of the chimpanzee pelvis and hind limb was developed that provides robust predictions of

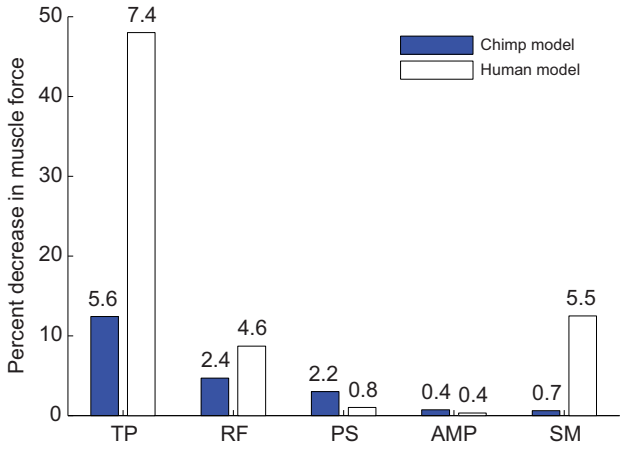

Fig. 7. Percent decrease in muscle force due to a 5% increase in tendon slack length. Dark bars are for the chimpanzee model and white bars are for a comparable human model (Arnold et al., 2010). All comparisons were made at the joint angle at which muscles produce peak force. The numbers located over each bar are the ratios of tendon slack length to optimal muscle fiber length. Muscles with a higher ratio tended to be more sensitive to changes in tendon slack length. With a few exceptions (e.g. m. psoas), the chimpanzee model had lower ratios of tendon slack length to muscle fiber length than the human model, and was therefore less sensitive to uncertainty in tendon slack length. The muscle–tendon unit names are abbreviated as: TP, m. tibialis posterior; SM, m. semimebranosus; RF, m. rectus femoris; PS, m. psoas; and AMP, m. adductor magnus proximal.

muscle–tendon unit moment arms over a wide range of joint motions (Fig. 1). The model is parameterized in large part based on cadaveric studies of the chimpanzee pelvis and hind limb musculoskeletal structure, allowing prediction of muscle–tendon unit length and force- and moment-generating capacities at the hip, knee and ankle.

Model predictions and sensitivities

The model moment arms corresponded well to the tendon-excursion measurements for the hip, knee and ankle muscles, suggesting that the model provides robust predictions of muscle–tendon unit moment arms over a wide range of joint positions (Fig. 3). Of course, perfect correspondence was not anticipated because some variation in muscle moment arm magnitude and pattern is to be expected within a species, and our chimpanzee model is based on a different individual than the ones used in Thorpe et al. (Thorpe et al., 1999), Payne et al. (Payne et al., 2006) and Holowka and O'Neill (Holowka and O'Neill, in press). The primary discrepancy we observed was the presence of higher-order phenomena in most of the model predictions. The absence of these nonlinear trends in the Thorpe et al. (Thorpe et al., 1999) data set is surprising, because moment arms are expected to vary as trigonometric functions of joint angle for many muscles. It is possible that the measurement technique used in Thorpe et al. (Thorpe et al., 1999), which included moment arm calculations at 10 deg intervals, may account for these patterns. Given this, moment arm studies that include instantaneous, simultaneous measurements of 3D kinematics and muscle–tendon displacements (cf. Delp et al., 1999; McCullough et al., 2011) are needed for chimpanzees. This is of particular importance for muscle–tendon units that are sensitive to joint positions outside the plane of interest, such as the musculature crossing the hip (cf. Fig. 8).

The muscle architecture data set used to parameterize the muscle–tendon units in our model reflects the best available data; however, at present these data are still rather limited. This is due to a range of factors, including the fact that the total number of chimpanzees studied to date is still quite small (Carlson, 2006; Holowka and O'Neill, in press; Myatt et al., 2011; Nagano, 2001; Thorpe et al., 1999) and that measurement techniques for determining optimal fascicle length based on the length of in-series sacromeres have not yet been applied (Lieber et al., 1994; Ward et al., 2009). Because of our assumption that the optimal fiber lengths in the model were equal to empirical fascicle length measurements,

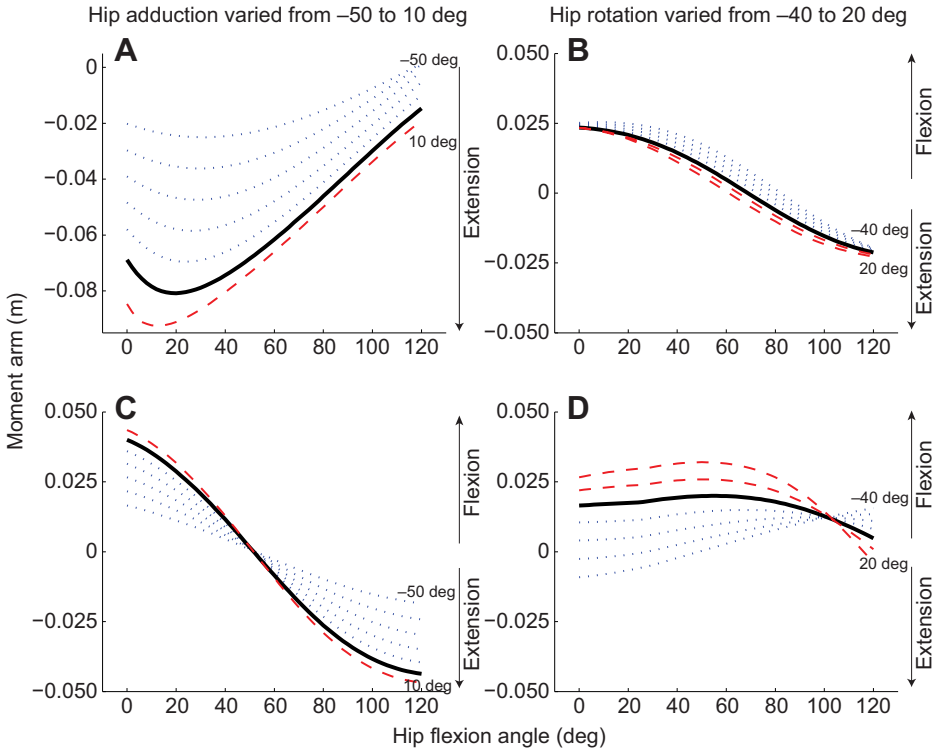

Fig. 8. The effects of changing hip adduction and hip rotation angles on flexion–extension moment arms for selected hip muscles. Solid lines represent moment arms with hip adduction and hip rotation set to 0 deg (i.e. neutral joint posture). Results are shown for (A) m. gluteus maximus proprius (caudal part), (B) m. pectineus, (C) m. adductor longus and (D) m. gluteus minimus (middle part). Dashed lines represent moment arms with the hip adducted (A,C) or medially rotated (B,D). Dotted lines represent moment arms with the hip abducted (A,C) or laterally rotated (B,D). Adduction and rotation joint angles were varied in 10 deg increments. The ordinate was set to the same range (0.1 m) in all panels to facilitate comparisons across muscles.

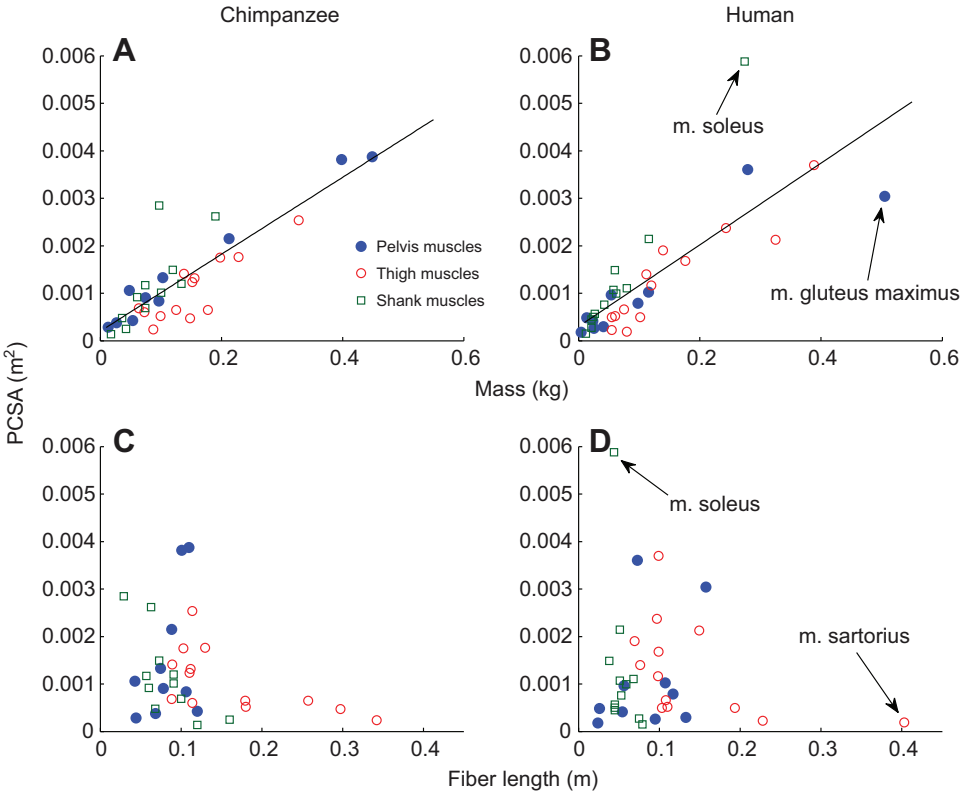

Fig. 9. Scatterplots of physiological cross-sectional area (PCSA) *versus* muscle mass for (A) the chimpanzee model and (B) a comparable human model, and scatterplots of PCSA *versus* optimal muscle fiber length for (C) the chimpanzee model and (D) the human model. Muscles with multiple paths in the model (e.g. m gluteus maximus) were combined for the purposes of data presentation. The dependence of PCSA on muscle mass and fiber length was similar between species. The slope of the least-squares regression line was 0.0081 (P<0.001, r^2=0.73) for the chimpanzee data (A) and 0.0086 (P<0.001, r^2=0.65) for the human data (B). The proportion of variance explained in the human model was slightly lower because of a small number of outliers. The greatest outliers in the human data set for PCSA *versus* mass were the m. soleus, with a relatively large PCSA for its mass, and the m. gluteus maximus, with a relatively small PCSA for its mass. The primary outliers for PCSA *versus* fiber length were the m. soleus, with a relatively large PCSA, and the m. sartorius, with relatively long fibers. Human data are from the musculoskeletal model of Arnold et al. (Arnold et al., 2010).

scaled to account for body size, some muscles may generate force over a different range of joint angles than predicted here. Clearly, more detailed studies of chimpanzee muscle are needed. Such data would have the potential to improve both active and passive muscle force and moment estimation, as well as provide additional insight into how muscles operate *in vivo* with respect to their force–length and force–velocity properties.

The ratios of peak strength predicted by the chimpanzee model for the hip and knee joints were generally similar to data from human studies (Anderson et al., 2007). The hip extension-to-flexion strength ratio in the model (1.9) was slightly greater than in humans (1.4), while the knee extension-to-flexion strength ratio in the model (1.6) was slightly lower than in humans (1.9). However, the results for the ankle joint differed considerably between species. The peak ankle plantar flexion moment predicted by the chimpanzee model was 6.6 times greater than the peak ankle dorsiflexion moment. In humans, the plantar flexors are also stronger than the dorsiflexors, but only by 3.0 to 3.5 times (Anderson et al., 2007; Marsh et al., 1981; Sale et al., 1982). The results for the chimpanzee model were because of both relatively weak dorsiflexors and relatively strong plantar flexors (based on PCSA) when compared with data from humans (Ward et al., 2009). Nevertheless, the total maximum isometric joint moments predicted at the hip, knee and ankle all exceed inverse dynamic estimates of the peak joint moments in chimpanzee bipedal and quadrupedal walking (Yamazaki, 1985; Thorpe et al., 2004; see also Sockol et al., 2007), suggesting that the chimpanzee model is sufficiently strong to simulate locomotion. Further, the plateaus of the hip, knee and ankle extension strength curves (Fig. 4) appear to correspond with mid-stance joint angles employed during locomotion in the pygmy chimpanzee, *Pan paniscus* (D'Août et al., 2002). Corresponding kinematic data for *P. troglodytes* are not available, at present.

A general finding from the systematic variation of muscle–tendon path parameters was that perturbing the locations of proximal muscle–tendon attachment points (origins and proximal via points) had relatively minor effects on muscle moment arms (Fig. 5). In contrast, muscle moment arms tended to be more sensitive to the locations of muscle–tendon insertion points. These results were due to the insertion points generally lying closer to the axes of rotations than the more proximal points. Therefore, moving an insertion point by a given amount tends to displace the muscle line-of-action more relative to the joint center than does moving an origin or proximal via point by the same amount. This is fortunate from a model development standpoint, as there is often more uncertainty in muscle origin locations than there is for insertions. This is especially true for muscles that have broad proximal attachments but terminate distally *via* a more focused tendon (e.g. m. gluteus medius and m. gluteus minimus). The greater sensitivity to insertion positions is closely related to the notion that peak muscle moment arms are correlated with the shorter distance between the joint axis and the origin or insertion (Murray et al., 2002). For muscles in the chimpanzee hind limb, the shorter distance will usually be to the insertion, thus the greater sensitivity to insertion placement is to be expected. The main exceptions will be in certain biarticular muscles. For example, the m. gastrocnemius lateralis moment arm at the knee joint will be more sensitive to uncertainty in the origin, rather than the insertion. Fortunately, the major biarticular muscles tend to have well-defined areas of attachment.

It is possible, in some circumstances, to precisely digitize the outline of the area of muscle attachment during a dissection, and then calculate the centroid of the area. Such an approach may be especially useful for muscles with broad proximal attachments. However, the effort involved in such a procedure may be unnecessary in many cases. This is for two reasons. First, our results show that moment arms are not especially sensitive to the location

of the point chosen for the origin. Second, the proper origin point for muscles with broad attachments is not actually a fixed point at the centroid of the attachment area, but rather the center of force application, which varies with motor unit recruitment *in vivo* (Monti et al., 2001).

Consistent with previous studies, model force- and moment-generating capacities were most sensitive to uncertainty in tendon slack lengths (Delp et al., 1990; Out et al., 1996; Redl et al., 2007), although the magnitude of the effect varied across muscles (Figs 6, 7). The different sensitivities were due in large part to differences in the ratio of tendon length to muscle fiber length (Table 2), though model sensitivity may be influenced by other geometric factors, such as the ratio of tendon length or muscle fiber length to moment arm (Delp et al., 1990). Unlike the maximum isometric force, optimal fiber length and pennation angle parameters in the muscle model, which may be based on muscle architecture measurements, tendon slack length does not have an easily measurable analog, as it includes both the external and internal portions of the tendon, as well as other sources of series elasticity. The numerical optimization approach used in the present study (from Manal and Buchanan, 2004) provided a systematic and uniform approach for determining tendon slack lengths that takes into account the operating range and optimal fiber length for each individual muscle. The sensitivities of optimal fiber length and tendon slack length are not completely independent of each other, as the muscle fiber and tendon lie in series, and together with pennation angle determine muscle–tendon length (Fig. 2). The tendon slack length optimization approach has the added effect of partially compensating for uncertainty in optimal fiber length. In Fig. 6B, optimal fiber lengths were perturbed without adjusting tendon slack length. However, we found that if the tendon slack length optimization was re-run after perturbing optimal fiber lengths, the effects on the predicted joint moment were reduced considerably (up to approximately 50%).

The ratios of tendon slack length to muscle fiber length in the chimpanzee model were generally smaller than in the human musculoskeletal model of Arnold et al. (Arnold et al., 2010). In addition to the chimpanzee model being less sensitive to uncertainty in tendon slack length, the smaller tendon to muscle fiber length ratios in the chimpanzee model may also have functional implications. Muscles with long tendons and short fibers are suitable for storage and release of elastic strain energy (Biewener and Roberts, 2000). The smaller tendon length to muscle fiber length ratios predicted in the chimpanzee model implies that chimpanzees have less potential for elastic energy utilization than humans. This may be an important contributing factor to the higher cost of transport in chimpanzees (Sockol et al., 2007), as storage and release of passive elastic energy functions as a metabolic cost-saving mechanism in terrestrial locomotion (e.g. Fukunaga et al., 2001; Umberger, 2010).

The systematic variation of hip joint angles about all three axes revealed that for some muscles, their function with respect to a particular joint axis depended heavily on the angle about one or both of the other hip joint axes (Fig. 8). This was true, for example, in the m. gluteus maximus proprius (caudal part), in that the hip extension moment arm could be varied more than fourfold by abducting the hip. Other muscles, such as the m. pectineus (Fig. 8), were far less sensitive to changes in the other hip joint angles. For both simplicity and consistency, the flexion–extension moment arms reported for the model in Fig. 3 were generated with hip adduction and rotation both set to the neutral position (0 deg). It should be kept in mind then, that for some muscle–tendon units, the degree of agreement with the experimental data could be improved, and for other muscle–tendon units worsened, by manipulating the hip adduction or rotation angles.

Limitations of the model validation

Our model provides accurate predictions of muscle moment arms and muscle–tendon unit lengths within the joint ranges of motion established for the model. However, outside of these ranges, its accuracy is undefined and may be reduced. Measurements of chimpanzee hind limb kinematics during walking, climbing and jumping (e.g. Isler, 2005; Scholz et al., 2006; Sockol et al., 2007) indicate that the joint ranges of motion in the model subsume several important muscle-powered movements. As such, the current limits on the joint ranges of motion should be adequate for most locomotor applications.

At present, it is not possible to validate the model predictions for abduction–adduction and internal–external rotation at the hip, as the available data are limited to flexion–extension moment arms. Although the magnitude and direction of the cadaveric moment arms at the hip fit well with model predictions for most muscles, it is clear that for some muscles (e.g. gluteal and adductor muscles) the 3D orientations of the pelvis and thigh segments during tendon-excursion experiments can have a significant effect on moment arm metrics. This may account for the discrepancies between the experimental measurements and model predictions for some muscles, such as the m. adductor longus; however, the degree of abduction–adduction and internal–external rotation of the cadaveric specimen of Thorpe et al. (Thorpe et al., 1999) and Payne et al. (Payne et al., 2006) are unknown.

Chimpanzee *versus* human muscle architecture

In the chimpanzee model, the muscles with the largest PCSAs were the m. gluteus maximus, m. tibialis posterior, m. soleus and m. vastus lateralis. For humans, the muscles with the largest PCSAs were the m. soleus, m. vastus lateralis, m. gluteus medius and m. gluteus maximus. This substantial overlap reflects the need in both species to generate extensor moments at the hip, knee and ankle to resist gravitational and inertial forces. The muscles with the greatest absolute PCSA in each species, the m. gluteus maximus in chimpanzees and the m. soleus in humans, correspond well with the functional demands of locomotion. Hip extension is the largest moment generated by chimpanzees in quadrupedal locomotion, while ankle plantar flexion is the largest moment generated in human walking (Sockol et al., 2007). The large PCSA for the m. tibialis posterior in chimpanzees may reflect its dual role as a plantar flexor and inverter, which is likely important in arboreal locomotion. The muscles with the longest fibers, the m. sartorius, m. gracilis and m. semitendinosus, were the same in chimpanzees and humans. These muscles are all knee flexors, while also functioning at the hip joint, which necessitates long fibers to accommodate large excursions (Ward et al., 2009).

The manner in which PCSA varies with muscle mass and fiber length in the chimpanzee model was similar to a comparable human model (Arnold et al., 2010). One of the major difference between species is the presence of an extreme muscle architecture in the m. soleus in humans, which favors high PCSA, and hence high force production. This relatively high PCSA is achieved through a moderately large mass and especially short fibers (Ward et al., 2009), as well as a medial expansion onto the tibia. In chimpanzees, the m. soleus has a robust PCSA, but not out of proportion with other lower limb muscles. The differences in m. soleus architecture between humans and chimpanzees seem to reflect the demands placed on this key muscle in different forms of locomotion. Human

bipedal locomotion requires substantial force production from the ankle plantar flexors (Komi et al., 1992). However, these high forces are typically exerted through a limited range of motion, which allows muscle fibers to be short. In contrast, locomotion in chimpanzees includes an arboreal component that demands considerable joint excursion, and therefore longer muscle fibers. This effectively limits muscle force capacity unless muscle mass is increased substantially. The architecture exhibited by the m. soleus in humans appears to be an adaptation for meeting the demands of our unique form of bipedalism. While taken to the extreme in the case of the m. soleus, the emphasis on joint excursion in chimpanzees and force production in humans is part of a more general trend noted by Thorpe et al. (Thorpe et al., 1999) and others (Payne et al., 2006; Holowka and O'Neill, in press).

Model use and future development

Musculoskeletal models are most powerful when integrated with a rich set of experimental data. Although numerous experimental studies over the past 75 years have investigated chimpanzee locomotion, there is still a great deal to be learned about the basic function of their bones, muscles and tendons during movement.

The 3D musculoskeletal model of the chimpanzee pelvis and hind limb presented here represents an important step in integrating experimental data on the mechanics, energetics and control of locomotor performance. An essential element of the model is that it permits detailed parameterization of the skeletal, muscle–tendon and neural systems. While much simpler models, such as pendulums, mass springs and colliding masses, have provided valuable insights into the fundamental dynamics of various locomotor tasks (e.g. Cavagna et al., 1977; Ruina et al., 2005), more complex models such as ours are needed to investigate the functional roles of specific details of bone and muscle (Delp et al., 1990; Neptune et al., 2009; Pandy, 2003; Umberger and Rubenson, 2011). Indeed, from the standpoint of trait evolution, detailed musculoskeletal models can be of considerable heuristic value, as it is almost impossible to assess the contribution of subtle changes in bone size and shape, muscle–tendon origins and insertions, or muscle architectural parameters on the global performance of the hind limb when that trait is studied in isolation. The extent to which the musculoskeletal morphologies of chimpanzees and humans reflect differences in locomotor capabilities is essential information for comparative studies of hominin fossil remains (e.g. Aiello and Dean, 1990; Lovejoy et al., 2009; Richmond and Jungers, 2008; Robinson, 1972; Stern and Susman, 1983; Zipfel et al., 2011). The use of detailed musculoskeletal models in combination with forward dynamics simulation and numerical optimization procedures provides a reproducible, mechanics-based approach for gaining insights into the relative importance of these different variables for a given muscle-driven task.

The extensible nature of our model allows further development of the underlying musculoskeletal structure (e.g. the addition of trunk, upper limb and head anatomy; intrinsic foot musculature) as well as implementation of inverse or forward dynamics analyses, based on experimental data, numerical optimization or some combination thereof. In this regard, validation of optimization criteria for predicting movement tasks in humans and chimpanzees is crucial if these same criteria are applied to fossil hominins or other species for performance-based prediction when experimental data are unavailable (e.g. Nagano et al., 2005; Sellers et al., 2005). As such, the model can also operate as a hypothesis generator for direct experimentation, and allow estimation of parameter values that are simply not feasible to measure directly.

ACKNOWLEDGEMENTS

Thanks to E. Delson and the staff at the American Museum of Natural History for support and assistance in arranging the loan of the chimpanzee skeleton used to build our model. Thanks also to K. Baab, D. Boyer, J. Groenke, B. Patel, J. Sertich and R. Susman for help with CT scanning and digital reconstruction.

AUTHOR CONTRIBUTIONS

M.C.O., S.G.L., B.D., J.T.S. and B.R.U. conceived of the model and the analyses. M.C.O., L.-F.L. and B.R.U. developed and tested the model. M.C.O., L.-F.L., S.G.L., B.D., J.T.S. and B.R.U. interpreted results obtained from the model. M.C.O., L.-F.L. and B.R.U. prepared the manuscript. S.G.L., B.D. and J.T.S. helped revise the manuscript.

COMPETING INTERESTS

No competing interests declared.

FUNDING

This study was supported by the National Science Foundation (BCS 0935327 and BCS 0935321).

REFERENCES

Aiello, L. and Dean, C. (1990). *An Introduction to Human Evolutionary Anatomy*. London: Academic Press.
Anderson, F. C. and Pandy, M. G. (2001). Dynamic optimization of human walking. *J. Biomech. Eng.* **123**, 381-390.
Anderson, D. E., Madigan, M. L. and Nussbaum, M. A. (2007). Maximum voluntary joint torque as a function of joint angle and angular velocity: model development and application to the lower limb. *J. Biomech.* **40**, 3105-3113.
Arnold, A. S. and Delp, S. L. (2001). Rotational moment arms of the medial hamstrings and adductors vary with femoral geometry and limb position: implications for the treatment of internally rotated gait. *J. Biomech.* **34**, 437-447.
Arnold, E. M. and Delp, S. L. (2011). Fibre operating lengths of human lower limb muscles during walking. *Philos. Trans. R. Soc. B* **366**, 1530-1539.
Arnold, E. M., Ward, S. R., Lieber, R. L. and Delp, S. L. (2010). A model of the lower limb for analysis of human movement. *Ann. Biomed. Eng.* **38**, 269-279.
Biewener, A. A. and Roberts, T. J. (2000). Muscle and tendon contributions to force, work, and elastic energy savings: a comparative perspective. *Exerc. Sport Sci. Rev.* **28**, 99-107.
Brown, I. E., Satoda, T., Richmond, F. J. and Loeb, G. E. (1998). Feline caudofemoralis muscle. Muscle fibre properties, architecture, and motor innervation. *Exp. Brain Res.* **121**, 76-91.
Carlson, K. J. (2006). Muscle architecture of the common chimpanzee (*Pan troglodytes*): perspectives for investigating chimpanzee behavior. *Primates* **47**, 218-229.
Cavagna, G. A., Heglund, N. C. and Taylor, C. R. (1977). Mechanical work in terrestrial locomotion: two basic mechanisms for minimizing energy expenditure. *Am. J. Physiol.* **233**, R243-R261.
D'Août, K., Aerts, P., De Clercq, D., De Meester, K. and Van Elsacker, L. (2002). Segment and joint angles of hind limb during bipedal and quadrupedal walking of the bonobo (*Pan paniscus*). *Am. J. Phys. Anthropol.* **119**, 37-51.
Delp, S. L. and Loan, J. P. (2000). A computational framework for simulating and analyzing human and animal movement. *IEEE Comput. Sci. Eng.* **2**, 46-55.
Delp, S. L., Loan, J. P., Hoy, M. G., Zajac, F. E., Topp, E. L. and Rosen, J. M. (1990). An interactive graphics-based model of the lower extremity to study orthopaedic surgical procedures. *IEEE Trans. Biomed. Eng.* **37**, 757-767.
Delp, S. L., Hess, W. E., Hungerford, D. S. and Jones, L. C. (1999). Variation of rotation moment arms with hip flexion. *J. Biomech.* **32**, 493-501.
Delp, S. L., Anderson, F. C., Arnold, A. S., Loan, P., Habib, A., John, C. T., Guendelman, E. and Thelen, D. G. (2007). OpenSim: open-source software to create and analyze dynamic simulations of movement. *IEEE Trans. Biomed. Eng.* **54**, 1940-1950.
Elftman, H. (1944). The bipedal walking of the chimpanzee. *J. Mammal.* **25**, 67-71.
Elftman, H. and Manter, J. (1935a). Chimpanzee and human feet in bipedal walking. *Am. J. Phys. Anthropol.* **20**, 69-79.
Elftman, H. and Manter, J. (1935b). The evolution of the human foot, with especial reference to the joints. *J. Anat.* **70**, 56-67.
Fitts, R. H., Bodine, S. C., Romatowski, J. G. and Widrick, J. J. (1998). Velocity, force, power, and Ca^{2+} sensitivity of fast and slow monkey skeletal muscle fibers. *J. Appl. Physiol.* **84**, 1776-1787.
Fukunaga, T., Kubo, K., Kawakami, Y., Fukashiro, S., Kanehisa, H. and Maganaris, C. N. (2001). In vivo behaviour of human muscle tendon during walking. *Proc. Biol. Sci.* **268**, 229-233.
Goodman, M. (1999). The genomic record of Humankind's evolutionary roots. *Am. J. Hum. Genet.* **64**, 31-39.
Hatze, H. (1977). A complete set of control equations for the human musculo-skeletal system. *J. Biomech.* **10**, 799-805.
Heiple, K. G. and Lovejoy, C. O. (1971). The distal femoral anatomy of *Australopithecus*. *Am. J. Phys. Anthropol.* **35**, 75-84.
Holowka N. B. and O'Neill M.C. (in press). Three-dimensional moment arms and architecture of chimpanzee (*Pan troglodytes*) leg musculature. *J. Anat.*
Ishida, H., Kumakura, H. and Kondo, S. (1985). Primate bipedalism and quadrupedalism: comparative electromyography. In *Primate Morphophysiology, Locomotor Analyses and Human Bipedalism* (ed. S. Kondo), pp. 59-80. Tokyo: University of Tokyo Press.

Isler, K. (2005). 3D-kinematics of vertical climbing in hominoids. *Am. J. Phys. Anthropol.* **126**, 66-81.
Jenkins, F. A., Jr (1972). Chimpanzee bipedalism: cineradiographic analysis and implications for the evolution of gait. *Science* **178**, 877-879.
Josephson, R. K. (1993). Contraction dynamics and power output of skeletal muscle. *Annu. Rev. Physiol.* **55**, 527-546.
Jungers, W. L., Meldrum, D. J. and Stern, J. T., Jr (1993). The functional and evolutionary significance of the human peroneus tertius muscle. *J. Hum. Evol.* **25**, 377-386.
Kimura, T. (1996). Centre of gravity of the body during the ontogeny of chimpanzee bipedal walking. *Folia Primatol.* **66**, 126-136.
Komi, P. V., Fukashiro, S. and Järvinen, M. (1992). Biomechanical loading of Achilles tendon during normal locomotion. *Clin. Sports Med.* **11**, 521-531.
Kumakura, H. (1989). Functional analysis of the biceps femoris muscle during locomotor behavior in some primates. *Am. J. Phys. Anthropol.* **79**, 379-391.
Latimer, B., Ohman, J. C. and Lovejoy, C. O. (1987). Talocrural joint in African hominoids: implications for *Australopithecus afarensis*. *Am. J. Phys. Anthropol.* **74**, 155-175.
Lieber, R. L., Loren. G. J. and Fridén, J. (1994). *In vivo* measurement of human wrist extensor muscle sarcomere length changes. *J. Neurophysiol.* **71**, 874-881.
Lovejoy, C. O., Suwa, G., Spurlock, L., Asfaw, B., White, T. D. (2009). The pelvis and femur of *Ardipithecus ramidus*: the emergence of upright walking. *Science*. **326**, 71e1-71e6.
Maganaris, C. N., Baltzopoulos, V., Ball, D. and Sargeant, A. J. (2001). In vivo specific tension of human skeletal muscle. *J. Appl. Physiol.* **90**, 865-872.
Manal, K. and Buchanan, T. S. (2004). Subject-specific estimates of tendon slack length: a numerical method. *J. Appl. Biomech.* **20**, 195-203.
Marsh, E., Sale, D., McComas, A. J. and Quinlan, J. (1981). Influence of joint position on ankle dorsiflexion in humans. *J. Appl. Physiol.* **51**, 160-167.
McCullough, M. B. A., Ringleb, S. I., Arai, K., Kitaoka, H. B. and Kaufman, K. R. (2011). Moment arms of the ankle throughout the range of motion in three planes. *Foot Ankle* **32**, 300-306.
Mendez, J. and Keys, A. (1960). Density and composition of mammalian muscle. *Metabolism* **9**, 184-188.
Mikkelsen, T. S., Hillier, L. W., Eichler, E. E. and Chimpanzee Sequencing and Analysis Consortium (2005). Initial sequence of the chimpanzee genome and comparison with the human genome. *Nature* **437**, 69-87.
Miller, R. H., Umberger, B. R., Hamill, J. and Caldwell, G. E. (2012). Evaluation of the minimum energy hypothesis and other potential optimality criteria for human running. *Proc. R Soc. B:* **279**, 1498-1505.
Modenese, L., Phillips, A. T. and Bull, A. M. (2011). An open source lower limb model: hip joint validation. *J. Biomech.* **44**, 2185-2193.
Monti, R. J., Roy, R. R. and Edgerton, V. R. (2001). Role of motor unit structure in defining function. *Muscle Nerve* **24**, 848-866.
Murray, W. M., Buchanan, T. S. and Delp, S. L. (2002). Scaling of peak moment arms of elbow muscles with upper extremity bone dimensions. *J. Biomech.* **35**, 19-26.
Myatt, J. P., Crompton, R. H. and Thorpe, S. K. S. (2011). Hindlimb muscle architecture in non-human great apes and a comparison of methods for analysing inter-species variation. *J. Anat.* **219**, 150-166.
Nagano, A. (2001). *A Computer Simulation Study of the Potential Locomotor Patterns of Australopithecus afarensis (A.L. 288-1)*. PhD dissertation, Arizona State University, Phoenix, AZ, USA.
Nagano, A., Umberger, B. R., Marzke, M. W. and Gerritsen, K. G. M. (2005). Neuromusculoskeletal computer modeling and simulation of upright, straight-legged, bipedal locomotion of *Australopithecus afarensis* (A.L. 288-1). *Am. J. Phys. Anthropol.* **126**, 2-13.
Narici, M. V., Maganaris, C. N., Reeves, N. D. and Capodaglio, P. (2003). Effect of aging on human muscle architecture. *J. Appl. Physiol.* **95**, 2229-2234.
Neptune, R. R., McGowan, C. P. and Kautz, S. A. (2009). Forward dynamics simulations provide insight into muscle mechanical work during human locomotion. *Exerc. Sport Sci. Rev.* **37**, 203-210.
Out, L., Vrijkotte, T. G., van Soest, A. J. and Bobbert, M. F. (1996). Influence of the parameters of a human triceps surae muscle model on the isometric torque-angle relationship. *J. Biomech. Eng.* **118**, 17-25.
Pandy, M. G. (2003). Simple and complex models for studying muscle function in walking. *Philos. Trans. R. Soc. B* **358**, 1501-1509.
Pandy, M. G., Zajac, F. E., Sim, E. and Levine, W. S. (1990). An optimal control model for maximum-height human jumping. *J. Biomech.* **23**, 1185-1198.
Payne, R. C., Crompton, R. H., Isler, K., Savage, R., Vereecke, E. E., Günther, M. M., Thorpe, S. K. S. and D'Août, K. (2006). Morphological analysis of the hindlimb in apes and humans. II. Moment arms. *J. Anat.* **208**, 725-742.
Redl, C., Gfoehler, M. and Pandy, M. G. (2007). Sensitivity of muscle force estimates to variations in muscle-tendon properties. *Hum. Mov. Sci.* **26**, 306-319.
Richmond, B. G. and Jungers, W. L. (2008). Orrorin tugenensis femoral morphology and the evolution of hominin bipedalism. *Science* **319**, 1662-1665.
Robinson, J. T. (1972). *Early Hominid Posture and Locomotion.* Chicago, IL: University of Chicago Press.
Rodman, P. S. and McHenry, H. M. (1980). Bioenergetics and the origin of hominid bipedalism. *Am. J. Phys. Anthropol.* **52**, 103-106.
Ruina, A., Bertram, J. E. A. and Srinivasan, M. (2005). A collisional model of the energetic cost of support work qualitatively explains leg sequencing in walking and galloping, pseudo-elastic leg behavior in running and the walk-to-run transition. *J. Theor. Biol.* **237**, 170-192.
Sale, D., Quinlan, J., Marsh, E., McComas, A. J. and Belanger, A. Y. (1982). Influence of joint position on ankle plantarflexion in humans. *J. Appl. Physiol.* **52**, 1636-1642.
Schmitt, D. (2003). Insights into the evolution of human bipedalism from experimental studies of humans and other primates. *J. Exp. Biol.* **206**, 1437-1448.
Scholz, M. N., D'Août, K., Bobbert, M. F. and Aerts, P. (2006). Vertical jumping performance of bonobo (*Pan paniscus*) suggests superior muscle properties. *Proc. R. Soc. B* **273**, 2177-2184.
Sellers, W. I., Cain, G. M., Wang, W. and Crompton, R. H. (2005). Stride lengths, speed and energy costs in walking of *Australopithecus afarensis*: using evolutionary robotics to predict locomotion of early human ancestors. *J. R. Soc. Interface* **2**, 431-441.
Sockol, M. D., Raichlen, D. A. and Pontzer, H. (2007). Chimpanzee locomotor energetics and the origin of human bipedalism. *Proc. Natl. Acad. Sci. USA* **104**, 12265-12269.
Stern, J. T., Jr (1972). Anatomical and functional specializations of the human gluteus maximus. *Am. J. Phys. Anthropol.* **36**, 315-339.
Stern, J. T., Jr (2000). Climbing to the top: a personal memoir of *Australopithecus afarensis*. *Evol. Anthropol.* **9**, 113-133.
Stern, J. T., Jr and Larson, S. G. (1993). Electromyographic study of the obturator muscles in non-human primates: Implications for interpreting the obturator externus groove of the femur. *J. Hum. Evol.* **24**, 403-427.
Stern, J. T., Jr and Susman, R. L. (1981). Electromyography of the gluteal muscles in *Hylobates*, *Pongo*, and *Pan*: implications for the evolution of hominid bipedality. *Am. J. Phys. Anthropol.* **55**, 153-166.
Stern, J. T., Jr and Susman, R. L. (1983). The locomotor anatomy of *Australopithecus afarensis*. *Am. J. Phys. Anthropol.* **60**, 279-317.
Swindler, D. R. and Wood, C. D. (1982). *An Atlas of Primate Gross Anatomy: Baboon, Chimpanzee, and Man*. New York, NY: Krieger Publishing.
Tardieu, C. (1983). *L'Articulation Du Genou: Analyse Morpho Fonctionnelle Chex Les Primates Application Aux Hominidés Fossils.* Paris: Centre National de la Recherche Scientifique.
Tardieu, C. (1992). *Le Centre De Gravité Du Corps Et Sa Trajectoire Pendant La Marche: Évolution De La Locomotion Des Hommes Fossiles.* Paris: Centre National de la Recherche Scientifique.
Taylor, C. R. and Rowntree, V. J. (1973). Running on two or on four legs: which consumes more energy? *Science* **179**, 186-187.
Thorpe, S. K. S., Crompton, R. H., Günther, M. M., Ker, R. F. and McNeill Alexander, R. (1999). Dimensions and moment arms of the hind- and forelimb muscles of common chimpanzees (*Pan troglodytes*). *Am. J. Phys. Anthropol.* **110**, 179-199.
Thorpe, S. K. S., Crompton, R. H. and Wang, W. J. (2004). Stresses exerted in the hindlimb muscles of common chimpanzees (*Pan troglodytes*) during bipedal locomotion. *Folia Primatol.* **75**, 253-265.
Tuttle, R. H., Basmajian, J. V. and Ishida, H. (1979). Activities of pongid thigh muscles during bipedal behavior. *Am. J. Phys. Anthropol.* **50**, 123-136.
Uhlmann, V. K. (1968). *Hüft- und Oberschenkelmuskulatur Systematische und vergleichende Anatomie*. Basel: S. Karger.
Umberger, B. R. (2010). Stance and swing phase costs in human walking. *J. R. Soc. Interface* **7**, 1329-1340.
Umberger, B. R. and Rubenson, J. (2011). Understanding muscle energetics in locomotion: new modeling and experimental approaches. *Exerc. Sport Sci. Rev.* **39**, 59-67.
Van der Helm, F. C., Veeger, H. E., Pronk, G. M., Van der Woude, L. H. and Rozendal, R. H. (1992). Geometry parameters for musculoskeletal modelling of the shoulder system. *J. Biomech.* **25**, 129-144.
Ward, S. R., Eng, C. M., Smallwood, L. H. and Lieber, R. L. (2009). Are current measurements of lower extremity muscle architecture accurate? *Clin. Orthop. Relat. Res.* **467**, 1074-1082.
Yamazaki, N. (1985). Primate bipedal walking: Computer simulation. In *Primate Morphophysiology, Locomotor Analyses and Human Bipedalism* (ed. S. Kondo), pp. 105-130. Tokyo: University of Tokyo Press.
Zajac, F. E. (1989). Muscle and tendon: properties, models, scaling, and application to biomechanics and motor control. *Crit. Rev. Biomed. Eng.* **17**, 359-411.
Zajac, F. E., Neptune, R. R. and Kautz, S. A. (2002). Biomechanics and muscle coordination of human walking. Part I: introduction to concepts, power transfer, dynamics and simulations. *Gait Posture* **16**, 215-232.
Zipfel, B., DeSilva, J. M., Kidd, R. S., Carlson, K. J., Churchill, S. E. and Berger, L. R. (2011). The foot and ankle of *Australopithecus sediba*. *Science* **333**, 1417-1420.